AIAA JOURNAL
Vol. 37, No. 12, December 1999

Nonlinear Structural Response of Laminated Composite Plates Subjected to Blast Loading

Halit S. Türkmen* and Zahit Mecitoglu†
Istanbul Technical University, 80626 Istanbul, Turkey

We are concerned with the theoretical analysis of the laminated composite plates exposed to normal blast shock waves as well as presenting correlation between the theoretical analysis and the experimental results of the strain time histories. The laminated composite plate is clamped at all edges. On the theoretical side of the study, dynamic equations of the plates are derived by the use of the virtual work principle within the framework of the Love theory of plates. The geometric nonlinearity effects are taken into account with von Kármán assumptions. Then the governing equations of the laminated plate are solved by the Runge–Kutta–Verner method. A new displacement function is considered for the theoretical solution of the blast-loaded clamped plate. Furthermore, finite element modeling and analysis for the blast-loaded composite plates are presented. On the experimental side of the study, tests have been carried out on the laminated composite plates with clamped edges for two different blast loads. The results of theoretical and finite element methods are compared with the experimental results. Theoretical and finite element analyses results are in a good agreement. There is a qualitative agreement between the analyses and experimental results in the first load case. The predicted peak strains and response frequency are in an agreement with the experimental results for first load case. Thus the theoretical solution may be used for providing material in the preliminary design stage. There is a difference between the analysis and experimental results in the second load case because of the extremely large deflections. In this study the effects of loading conditions, geometrical properties, and material properties are separately examined on the dynamic behavior, as well.

Nomenclature

a, b	= dimensions of the plate
d	= distance from open end of the tube to target plate
E_1, E_2	= Young's moduli
G_{12}	= shear modulus
h	= plate thickness
h_k	= ply thickness
J_e	= virtual work
M_x, M_y, M_{xy}	= stress couples
m, n	= term numbers
$\bar{m}$	= unit area mass of plate
N_x, N_y, N_{xy}	= stress resultants
p	= pressure
p_c	= constant portion of the peak pressure
p_m	= peak pressure
Q_{ij}	= elastic constant components for a laminated composite ($i = 1, 2, 6;\ j = 1, 2, 6$)
q_x, q_y, q_z	= load components
t	= time
t_p	= positive phase duration
U, V, W	= time-dependent parts of displacement components
u, v, w	= displacement components in the x, y, z directions
u^0, v^0, w^0	= displacement components of reference surface in the x, y, z directions
$\dot{u}, \dot{v}, \dot{w}$	= components of velocity vector
$\ddot{u}, \ddot{v}, \ddot{w}$	= components of acceleration vector
α	= waveform parameter
$\varepsilon_x, \varepsilon_y, \varepsilon_{xy}$	= strain components
$\kappa_x, \kappa_y, \kappa_{xy}$	= plate curvatures
ν_{12}	= Poisson's ratio
ρ	= density of material
$\sigma_x, \sigma_y, \sigma_{xy}$	= stress components

Received 9 April 1998; revision received 26 March 1999; accepted for publication 28 April 1999.

*Research Assistant, Aeronautics and Astronautics Faculty; currently Postdoctoral Associate, Mechanical and Aerospace Engineering Department, Cornell University, 258 Upson Hall, Ithaca, NY 14853.

†Professor, Aeronautics and Astronautics Faculty.

I. Introduction

ADVANCED composites are being used in many applications ranging from aircraft and submarines to pressure vessels and automotive parts. For instance, aircraft interior panels, aircraft cargo liners, aircraft brakes, ballistic components, launch systems, self-contained space modules, sports equipment, naval vessels, medical equipment, rail cars, trains, strategic and tactical missiles are some of the distinctive fields of application mentioned in the literature.[1] In all of these applications the laminated composite plate components are being subjected to different loading conditions. Among them air-blast load is of significant importance. The air-blast load, which is one type of extraordinary dynamic load, is produced as a consequence of explosion.

The assessment of the effects of the explosives on structural systems was apparently not studied systematically until World War I. The early published work was Hopkinson's study,[2] in which he outlined his theory for using scale models with the statement: "If two structural systems, identically similar except in size, be subjected to blast loading from two explosive charges whose weights are in proportion to the cube of the ratio of the linear dimensions of the two structures, then the behavior of the two structural systems will be identically similar with the distortions scaling as the ratio of the linear dimensions."

There are some studies related to isotropic panel structures subjected to air-blast loading in the literature. The prediction and measurement of the structural response of ship panels to free field air-blast explosions were first investigated by Houlston et al.[3] In the research conducted by Houlston and DesRochers,[4] the square plates and stiffened panels subjected to air-blast and underwater shock loads were investigated. Later, assuming a Navier form of displacement function and a modified Friedlander reflected blast overpressure loading that exponentially decays with time, Gupta et al.[5] conducted a single-degree-of-freedom elastodynamic analysis of the response of a rectangular plate subjected to an explosive blast. Beshara[6] investigated the prediction of dynamic effects of unconfined explosions needed for the structural analysis of blast-loaded above-ground structures. New modeling methods for stiffened plates and cylindrical shell structures were presented by Olson.[7] In his study rigid plastic analysis was extended to orthogonally stiffened plates and investigations were conducted by introducing new efficient finite element and finite strip representations for stiffened plates and cylindrical shells, respectively. Experimental

and numerical results for fully built-in stiffened square plates subjected to blast pressure loading were presented by Nurick et al.[8] His numerical analysis was carried out by using a finite element formulation that incorporates nonlinear geometry and material effects as well as strain-rate sensitivity. Elastic and plastic design methods for lightweight metallic corrugated core sandwich panels subjected to air-blast loading were presented by Wiernicki et al.[9] In their paper the equations were offered as a set of relatively simple analytical expressions that can be used in preliminary design. There are a few studies related to laminated plates subjected to air-blast loading in the literature. Librescu and Nosier[10] in their theoretical analysis of the symmetrically laminated rectangular composite flat panels exposed to blast loading took into account the shear deformation effect. A theoretical and numerical study including the nonlinear effects was presented by Türkmen and Mecitoglu.[11] Recently, Türkmen et al.[12] carried out a numerical study on the dynamic behavior of laminated composite plates subjected to shock loading. Türkmen[13] investigated the dynamic behavior of composite plate and shell structures subjected to blast load. In his study the theoretical solution based on the Love theory is presented. The theoretical results are compared with the experimental and finite element results.

The specifically concerned area of investigation of this paper is the nonlinear geometric analysis of laminated plates subjected to blast loading. The Love theory of plates is used in the nonlinear range. In the theory the assumption is made that the plate is thin, transverse shear strains are neglected, and large deflections are included. The equation of motion is obtained by the use of the virtual work principle. The Runge–Kutta–Verner method is used to obtain the solution. In addition ANSYS finite element software is utilized for obtaining strain time history in the linear and nonlinear ranges. Experiments are carried out to test the laminated composite plates with clamped edges. A blast loading is obtained from the detonation wave, which is developed in a tube by the reaction of liquified petroleum gas (LPG) and oxygen mixtures. The numerical results are compared with the experimental ones, and an agreement is found. The effects of loading conditions, geometrical properties, and material properties are examined on the dynamic behavior.

II. Experimental Work

For obtaining the air-blast loading a detonation is developed from the reaction of LPG-oxygen mixture in a long circular cylindrical detonation tube. The detonation tube, the laminated composite plate, and the plate-mounting frame used in the tests are shown in Fig. 1. The detonation tube is fixed to two steel box beams, which are clamped to a concrete base seated on the ground. The plate-mounting frame is placed in front of the detonation tube. The mounting is designed with the object of providing clamped boundary conditions. The target plate is compressed between the two steel frames with

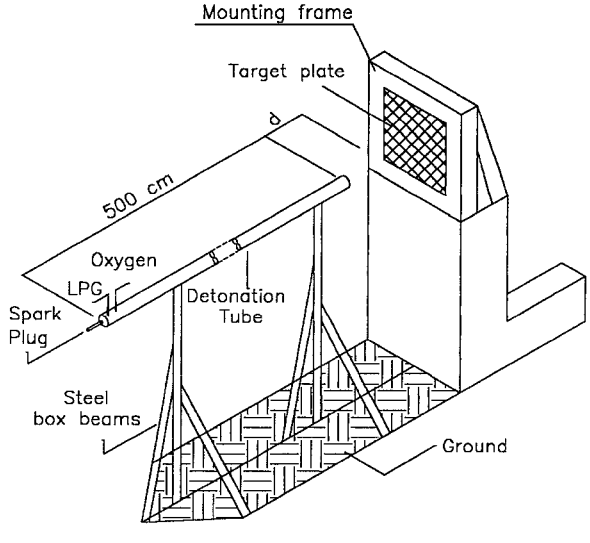

Fig. 1 Placement of the detonation tube, plate-mounting frame, and plate.

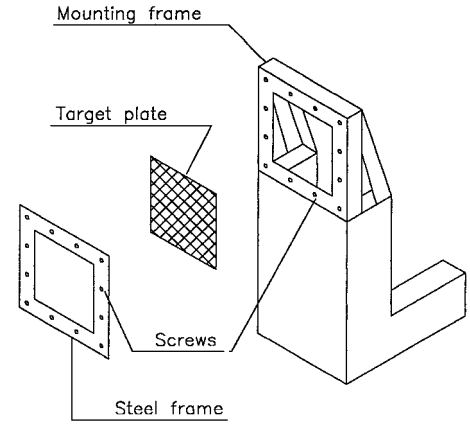

Fig. 2 Exploded view of the plate-mounting system.

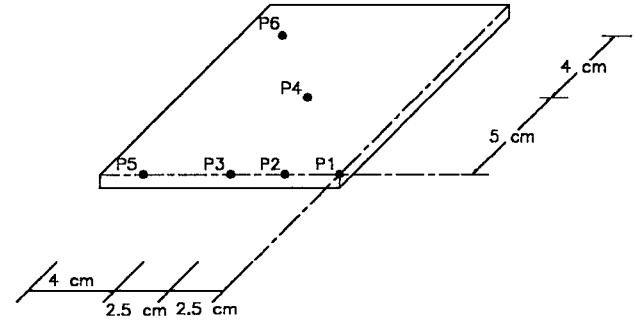

Fig. 3 Placement of the pressure transducers.

12 bolts, and so it is achieved that there are no displacements in the in-plane and out-of-plane directions on the boundaries in the tests. Figure 2 shows the details of the square plate-mounting frame used in the tests.

Blast-Pressure Measurement

The LPG and oxygen mixture are ignited in the detonation tube to obtain air-blast pressure load for which the plate is experienced against. The ratio of LPG-oxygen mixture and mass of the mixture are stabilized by using a computer. The detonation tube is centered with respect to plate to obtain a symmetrically distributed blast loading on the plate. The air-blast pressure distribution is obtained by using quartz crystal pressure transducers placed on the wooden model, which is exposed to the blast loading. Assuming the distribution of the blast loading on the target model is symmetrical, transducers are placed at six points on a quarter model (Fig. 3). The signal obtained from the transducer is amplified by using a charge amplifier. The air-blast pressure distribution is obtained for 35- and 100-cm distances from the detonation tube to investigate the effect of blast on the near and distant structures, respectively.

Strain Measurement

Strain gauges and Wheatstone bridge are used to obtain the dynamic strain. The strain gauge is mounted on the center of each plate in the x direction. The signal obtained from the bridge circuit is amplified and calibrated by using a dynamic strain meter.

The signal obtained from the charge amplifier and the dynamic strain meter are digitized by using a 100-MHz digital scope, and the data are transferred to a PC by using a RS232C serial interface. All processes to develop the detonation wave and the measurements of pressure and strain on the plates are controlled using a PCL818 card and a computer.

III. Nonlinear Dynamic Response Analysis

In this section the mathematical model of the laminated composite plate subjected to blast loading is presented. The resulting time-dependent equation is solved by Runge–Kutta–Verner method. The laminated composite plate and Cartesian coordinate system are depicted in the Fig. 4.

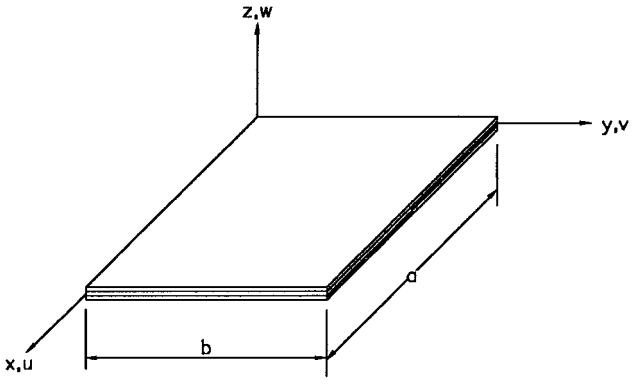

Fig. 4 Laminated plate and coordinate system.

Governing Equations

The displacement field in the plate can be represented by polynomials or trigonometric series.[14] The first few terms of the series expansion for the displacements u, v, and w are derived as[15]

$$u = u^0 + u^a(z/h) + u^s \sin(\pi z/h)$$

$$v = v^0 + v^a(z/h) + v^s \sin(\pi z/h)$$

$$w = w^0 + w^a(z/h) + w^c \cos(\pi z/h) \tag{1}$$

In classical plate theory the w^a term and the trigonometric terms are absent, and the terms u^a/h and v^a/h are replaced by $-\partial w^0/\partial x$ and $-\partial w^0/\partial y$, respectively. With this assumption strain-displacement relationships for the plate can be written as

$$\varepsilon_x = \varepsilon_x^0 + z\kappa_x, \qquad \varepsilon_y = \varepsilon_y^0 + z\kappa_y, \qquad \varepsilon_{xy} = \varepsilon_{xy}^0 + z\kappa_{xy} \tag{2}$$

where

$$\varepsilon_x^0 = \frac{\partial u^0}{\partial x} + \frac{1}{2}\left(\frac{\partial w^0}{\partial x}\right)^2, \qquad \kappa_x = -\frac{\partial^2 w^0}{\partial x^2}$$

$$\varepsilon_y^0 = \frac{\partial v^0}{\partial y} + \frac{1}{2}\left(\frac{\partial w^0}{\partial y}\right)^2, \qquad \kappa_y = -\frac{\partial^2 w^0}{\partial y^2}$$

$$\varepsilon_{xy}^0 = \frac{\partial u^0}{\partial y} + \frac{\partial v^0}{\partial x} + \frac{\partial w}{\partial x}\frac{\partial w}{\partial y}, \qquad \kappa_{xy} = -2\frac{\partial^2 w^0}{\partial x \partial y}$$

For an anisotropic material the constitutive equations can be expressed as[16]

$$\sigma_x = Q_{11}\varepsilon_x + Q_{12}\varepsilon_y + Q_{16}\varepsilon_{xy}$$

$$\sigma_y = Q_{21}\varepsilon_x + Q_{22}\varepsilon_y + Q_{26}\varepsilon_{xy}$$

$$\sigma_{xy} = Q_{61}\varepsilon_x + Q_{62}\varepsilon_y + Q_{66}\varepsilon_{xy} \tag{3}$$

The equations of motion are derived from the virtual work principle. For the thin laminated plates the response characteristics obtained within classical and shear deformable theories are in perfect agreement in linear range.[10] In this study the classical plate theory with von Kármán assumptions is used for nonlinear geometric analysis of thin laminated plates, theoretically. Transverse shear stresses, which have not been in the classical theory, are ignored in the theoretical analysis. Because the assumption is made that in-plane forces are small compared to the forces in the normal direction of the plate because of the blast effect, in-plane inertia are ignored. Thus, the virtual work principle is applied to the plate, and the following equation is obtained:

$$\delta J_e = \int_T \mathrm{d}t \iint_A (\sigma_x \delta\varepsilon_x + \sigma_y \delta\varepsilon_y + \sigma_{xy}\delta\varepsilon_{xy})\,\mathrm{d}A - \iint_A (q_x\delta u + q_y\delta v + q_z\delta w)\,\mathrm{d}A - \iint_A [\bar{m}(\dot{u}\delta\dot{u} + \dot{v}\delta\dot{v} + \dot{w}\delta\dot{w})]\,\mathrm{d}A = 0 \tag{4}$$

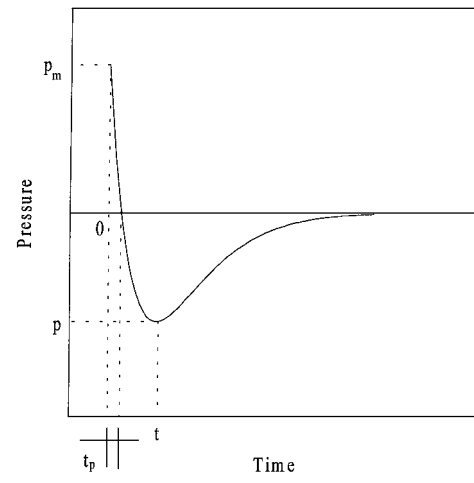

Fig. 5 Blast-pressure curve.

The equations of motion are derived, substituting the constitutive equations into the virtual work equation. The derivation of the equations of motion is given in the Appendix.

Blast Loading

The shock or blast wave is generated when the atmosphere surrounding the explosion is forcibly pushed back by the hot gases produced from the explosion source. The front of the wave, called the shock front, is like a wall of highly compressed air and has an overpressure much greater than that in the region behind it. This peak overpressure decreases rapidly as the shock is propagated outward. After a short time the pressure behind the front may drop below the ambient pressure, as shown in Fig. 5. During such a negative phase, a partial vacuum is created, and air is sucked in. The air-blast pressure on an exposed surface is a function of the air-blast pressure magnitude, and the orientation, geometry, and size of the surface that the shock wave encounters and distance from the detonation source. An approximation to the time variation of the blast pressure is given by the Friedlander decay function as

$$p(t) = p_m(1 - t/t_p)e^{-\alpha t/t_p} \tag{5}$$

Solution Method

The solution is assumed to be a multiplication of coordinate and time-dependent parts. With this assumption the displacement functions for clamped plate are given by the following functions:

$$u^0 = \sum_{m=1}^{M}\sum_{n=1}^{N} U_{mn}(t)\left(1 - \cos\frac{2m\pi x}{a}\right)\left(1 - \cos\frac{2n\pi y}{b}\right)$$

$$v^0 = \sum_{m=1}^{M}\sum_{n=1}^{N} V_{mn}(t)\left(1 - \cos\frac{2m\pi x}{a}\right)\left(1 - \cos\frac{2n\pi y}{b}\right)$$

$$w^0 = \sum_{m=1}^{M}\sum_{n=1}^{N} W_{mn}(t)\left(1 - \cos\frac{2m\pi x}{a}\right)\left(1 - \cos\frac{2n\pi y}{b}\right) \tag{6}$$

The Galerkin method is used to obtain the system of differential equations of motion, which is a function of time. Hence the Eqs. (A6) can be written in the following form:

$$\iint_A \left[L_{11}u^0 + L_{12}v^0 + L_{13}w^0 + N_1(w^0) + \bar{m}\ddot{u}^0 - q_x\right]u^0\,\mathrm{d}A = 0$$

$$\iint_A \left[L_{21}u^0 + L_{22}v^0 + L_{23}w^0 + N_2(w^0) + \bar{m}\ddot{v}^0 - q_y\right]v^0\,\mathrm{d}A = 0$$

$$\iint_A \left[L_{31}u^0 + L_{32}v^0 + L_{33}w^0 + N_3(u^0, v^0, w^0) + \bar{m}\ddot{w}^0 - q_z\right]w^0\,\mathrm{d}A = 0 \tag{7}$$

Because the panel is subjected to normal blast pressure, the loads in the x and y directions are equal to zero, and in-plane inertia are ignored. Therefore u^0 and v^0 are calculated from the first two of Eqs. (7) as zero. Thus the remainder of Eqs. (7) is written in the following form:

$$\iint_A \left[L_{33}w^0 + N_3(u^0, v^0, w^0) + \bar{m}\ddot{w}^0 - q_z\right]w^0 \, dA = 0 \qquad (8)$$

Integrating Eq. (8), the nonlinear differential equation of motion of the plate subjected to blast loading is obtained. The resulting equation is solved by the Runge–Kutta–Verner method.

Finite Element Analysis

In addition to the theoretical method, ANSYS finite element software is used to obtain strain time history numerically. The finite element model for the plate consists of an assembly of two-dimensional shell elements with seven layers in the transverse direction. In the finite element model no slippage is assumed between the element layers. Shear deflections are included in the element; however, normal to the center plane before deformation is assumed to remain straight after deformation. The stress varies linearly through the thickness of each layer. The plate is discretized by the use of eight-noded laminated shell elements. There are six degrees of freedom at each node. Three different models consisted of uniform grids with 16, 36, and 64 shell elements to verify the accuracy of the finite element model.[3] Comparison of the natural frequencies for the first mode shows a 2.5% decrease when changing the grid mesh from 16 to 36 elements and a 0.2% decrease when refining this grid from 36 to 64 elements. Convergence of the fundamental frequency shows that the mesh of 64 elements is sufficient to give adequate accuracy.

The pressure load is applied on the whole surface of the plate as a function of time. A total of 100 time function points are used in describing the exponentially decaying blast load. All edges of the plate are modeled by clamped boundary conditions. For the linear transient analysis of the plate, time integration is done using the Newmark method. On the other hand, the Newton–Raphson technique is used for the nonlinear transient analysis. Time increment is taken to be 0.1 ms in the linear and nonlinear analyses.

IV. Results and Discussion

In this study the blast loading is obtained from the detonation wave, which is developed in a tube by the reaction of LPG and oxygen mixtures. Then, the detonation wave goes through to atmosphere from the open end of the tube and applies a normal blast load on the target plate that is mounted at a distance from the open end of the tube.

Two different distances are experienced: 100 and 35 cm. Pressure transducers are mounted on a wooden model, and blast-pressure variation and distribution are obtained on the wooden model. Because the plate geometry and the blast-pressure effect are symmetrical according to two axes of symmetry, air-blast pressure is measured at six different points on a quarter wooden model. Blast measurements are repeated three times, and average values are calculated.

Pressure measurement results are shown in Tables 1 and 2 for 100- and 35-cm distances from the open end of the detonation tube, respectively. The spatial distribution of the peak pressure on the quarter model is shown in Fig. 6 for the 35-cm distance. The experimental results show that the distance is a very significant factor affecting the variation of air-blast pressure in spatial and time domains. The pressure is uniformly distributed for the distance of 100 cm according to blast test results. However, one can see that there is a variation in the readings from trial to trial from the transducers used to measure pressure. This variation is not considered in the analyses. However, this variation increases or decreases the predicted peak strain in the ratio of variation in linear range. The effect of this variation will be small in nonlinear range. The pressure has a sinusoidal variation for the 35-cm distance. Therefore a sinusoidal approximation to the spatial variation of peak pressure is considered, providing the experimental results. A sinusoidal approximation to peak pressure distribution obtained from the experiments is given in the same figure. The pressure-time variations measured at P1 point are shown in Figs. 7a and 7b for 100- and 35-cm distances from the open end of the tube, respectively. The magnitude and variation of the air-blast pressure changes by the distance. The ratio of the positive peak pressure to the negative peak pressure increases with the increasing distance. In the low distance case experimental results show that the blast load has a large negative peak pressure. The blast pressure variation, measured in the tests, show that the load suddenly increases and then exponentially decays with time. During the decaying of blast pressure, some pressure fluctuations are observed.

Table 1 Blast test results for 100-cm distance (bar)

Transducer	Test 1	Test 2	Test 3	P_{av}
1	0.287	0.290	0.289	0.289
2	0.286	0.302	0.285	0.291
3	0.289	0.277	0.311	0.292
4	0.267	0.285	0.298	0.283
5	0.312	0.288	0.322	0.307
6	0.254	0.297	0.295	0.282

Table 2 Blast test results for 35-cm distance (bar)

Transducer	Test 1	Test 2	Test 3	P_{av}
1	3.047	2.578	3.281	2.968
2	2.344	2.262	2.237	2.281
3	1.406	1.406	1.406	1.406
4	0.938	0.938	0.911	0.929
5	0.938	0.859	0.937	0.911
6	0.703	1.016	0.703	0.807

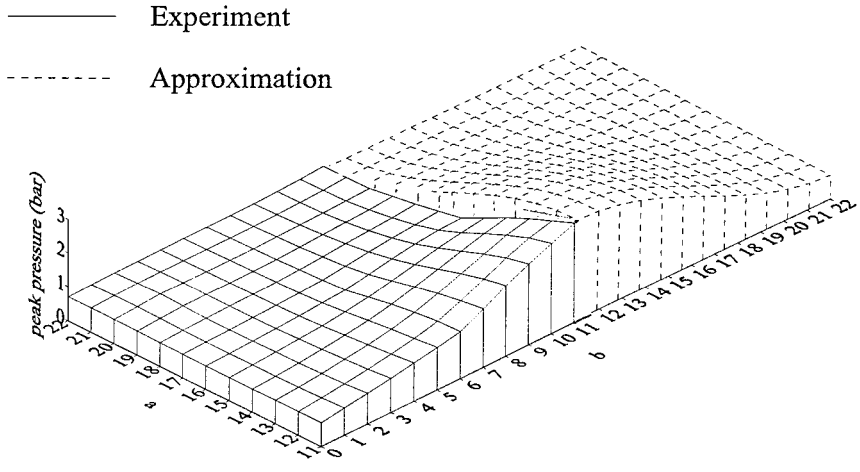

Fig. 6 Blast-pressure distribution on the plate.

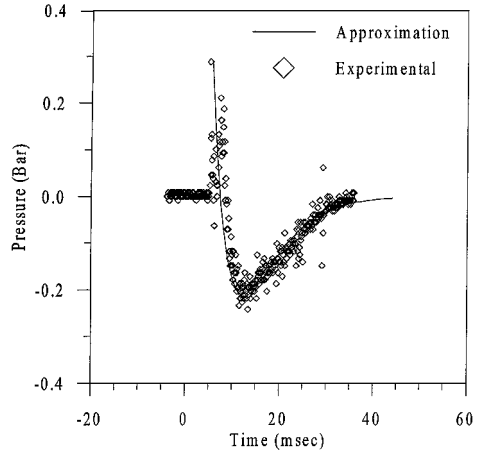

a) $d = 100$ cm

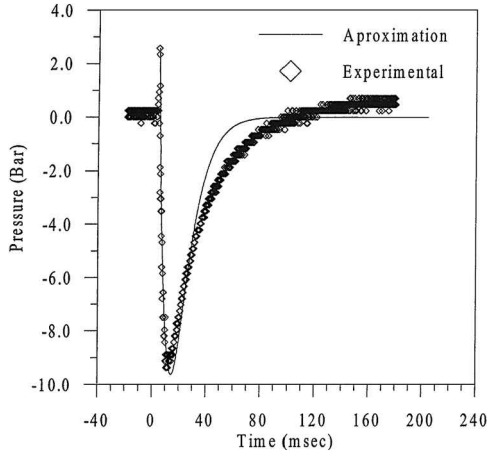

b) $d = 35$ cm

Fig. 7 Variation of blast loading by time.

An approximation to the time variation of pressure is given by Eq. (5) for the uniform distribution. Furthermore, multiplying the Friedlander decay function with sine functions, the spatial and time variation of the pressure is obtained as a function of time and coordinates for the distance of 35 cm. This relationship is expressed as

$$p(x, y, t) = \left[(p_m - p_c)\sin(\pi x/a)^2 \sin(\pi y/b)^2 + p_c\right](1 - t/t_p)e^{-\alpha t/t_p} \tag{9}$$

An acceptable approximation to the blast loading test results can be accomplished by choosing the appropriate values of p_m and t_p in Eq. (5) and then by calculating the waveform parameter α, in terms of them. In this study the values of p_m and t_p are chosen at negative peak pressure time (Fig. 5), and then the waveform parameter is determined. In Eq. (9) p_c is the peak pressure on the edge of the plate. Figures 7a and 7b show the approximate curves for the time variation of the pressure.

Two types of plates are used in the tests. One of them, labeled specimen I, is a seven-layered fiberglass fabric (90-deg/0-deg fiber orientation angle for one layer) whose thickness is 1.96 mm. The second plate, labeled specimen II, is a five-layered fiberglass fabric (45-deg/−45-deg fiber orientation angle for one layer) whose thickness is 1.2 mm. All layers are taken to be of equal thickness. The effective dimension of all of the square plates is 220 mm. The test specimens are made by hand lay-up technique. Glass fibers (181 style) are laid onto a mold by hand, and the AW106 resin is brushed on. The deposited layers are densified with rollers. Curing time is three days at room temperature. The vacuum, which is used in this process, is 736 mm Hg. The plain weave is used in the specimens. The weight ratios of the glass fabric and the resin to the composite are equal. Ply material properties used in the analysis and experiments are given as

$$E_1 = 24.14\,\text{GPa}, \qquad E_2 = 24.14\,\text{GPa}, \qquad G_{12} = 3.79\,\text{GPa}$$

$$\rho = 1800\,\text{kg/m}^3, \qquad \nu_{12} = 0.11$$

The test and analysis are performed for two different loading conditions, which are shown in Table 3. Theoretical, numerical, and experimental results of specimen I are obtained for the first loading condition. One-, four-, and nine-term series solution results show that the overall trend of the predicted plate response is not affected by the term number used in the linear theoretical analysis (Fig. 8); however, the results are affected as to small amplitude variations at higher frequencies. These small amplitude variations are shown in the four- and nine-term series solution results because the effect of higher vibration modes is taken into account by using more than one term in the analysis. Theoretical results are in a good agreement with the ANSYS results in the linear range (Fig. 9). In the nonlinear range finite element displacement results are in a good agreement with the nine-term series solution results (Fig. 10). The discrepancy between the strain time history results of the finite element and theoretical method is caused by the effect of the membrane strains

Table 3 Loading conditions

Parameters	Load case I	Load case II
p_m, N/m^2	28,906	296,875
p_c, N/m^2	0	70,000
d, cm	100	35
α	0.35	0.06
t_p, s	0.0018	0.0009
Pressure distribution	Uniform	Sinusoidal

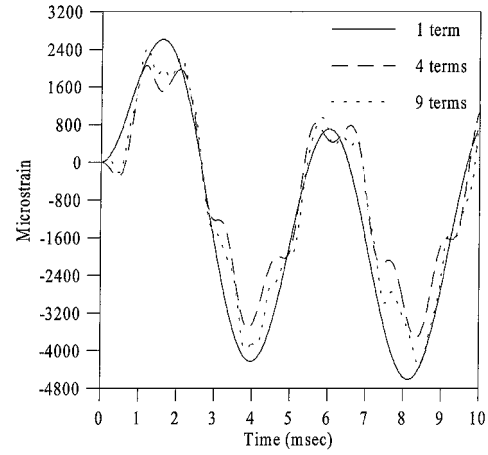

Fig. 8 Effect of the term number on the analysis.

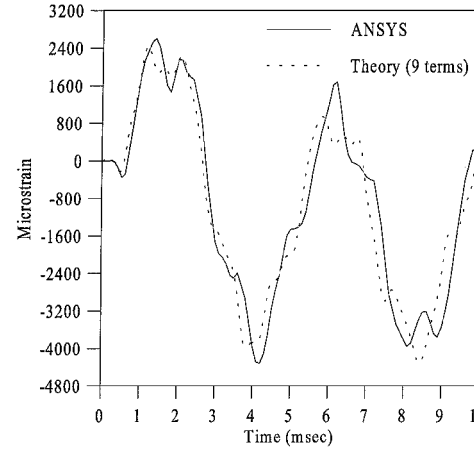

Fig. 9 Comparison of the strain time history results in the linear range.

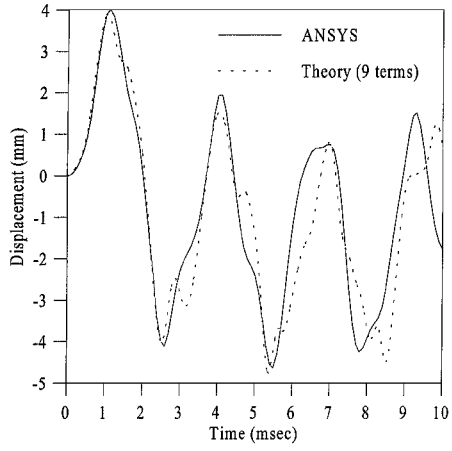

Fig. 10 Comparison of the displacement time history results in the nonlinear range.

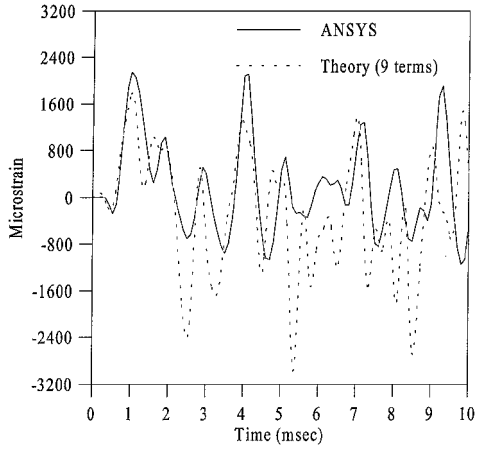

Fig. 11 Comparison of the strain time history results in the nonlinear range.

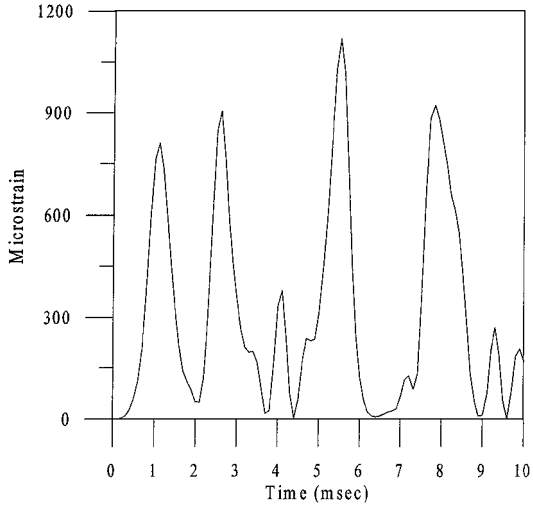

Fig. 12 Membrane strain time history results of specimen I under first loading condition.

(Fig. 11). Because of the geometric nonlinearities, large membrane strains occur. The membrane strain time history obtained by using ANSYS is shown in Fig. 12. In the theoretical analysis the first two of Eqs. (7) are ignored to simplify the solution, and so the membrane strains are ignored. These membrane strains increase the stiffness of the plate after the strain reaches the peak value. After the positive peak strain the negative pressure pulse increases the negative peak strain. The small negative peak strain is obtained in the numerical analysis because of the membrane strains. However, bigger negative peak strain is obtained from the theoretical analysis

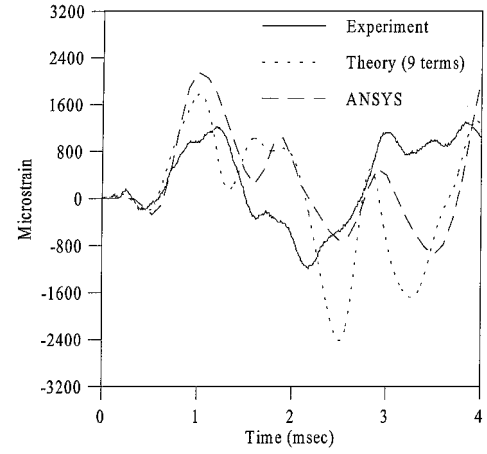

Fig. 13 Strain time history results.

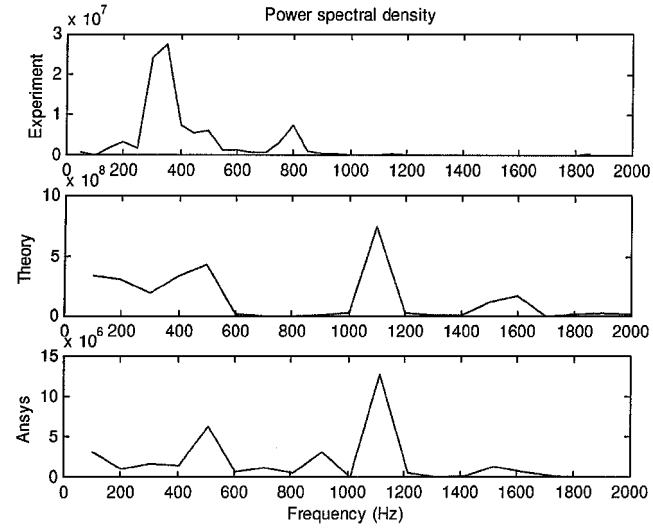

Fig. 14 Response frequencies.

because the membrane strains are ignored in this analysis. However, the predicted peak strain is well-correlated with the ANSYS results because the membrane strains are small in the beginning of the plate vibration. The wall-clock times, which we wait for solution, are given to compare the theoretical and numerical analyses costs. The wall-clock times are 4 and 117 min for the theoretical and numerical solution, respectively. The strain time history results obtained from theoretical, numerical, and experimental methods are compared in Fig. 13. The predicted peak strain value obtained from the nine-term series solution is well-correlated with the numerical result. A qualitative agreement is found between the theoretical, numerical, and experimental results. The fast Fourier transformation technique is used for obtaining the response frequency. The power spectral densities of the results, which is a measurement of the energy at various frequencies, are obtained for the theoretical, numerical, and experimental results of specimen I under the first loading condition. The spectral analysis results show that the frequencies obtained from theoretical and numerical methods are in an agreement. The primary frequency obtained from the experimental result is in agreement with the secondary frequency obtained from the theoretical and numerical results (Fig. 14). The discrepancy between the peak strains obtained from the experimental and the other methods is caused by assumptions made in the analyses. One of them is that no slippage is assumed between the element layers in both analyses. In the other assumption the higher-order nonlinear terms are ignored in the analyses. Considering the large deflection, the slippage between the element layers and higher-order nonlinear terms affects the results. The blast-load test results have pressure fluctuations, which are ignored in the analyses. The pressure fluctuations cause the difference between the experimental and analytic

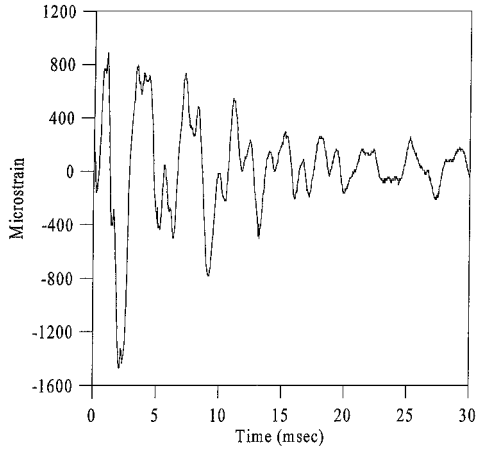

Fig. 15 Long-time response.

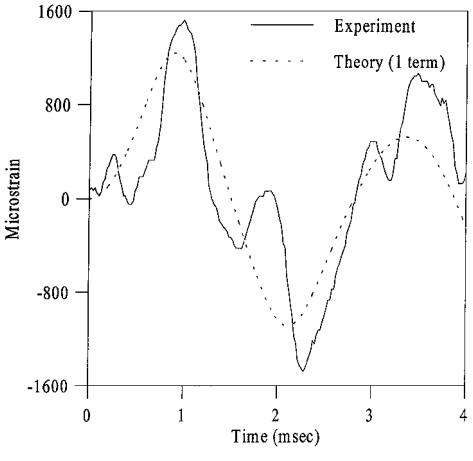

Fig. 16 Strain time history results for specimen II.

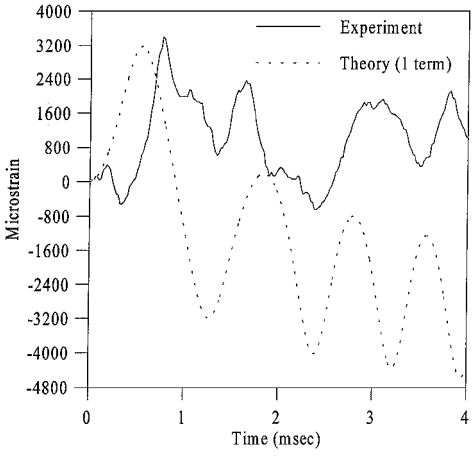

Fig. 17 Strain time history results for load condition II.

results. Furthermore, the damping effects decrease the vibration amplitude in a short time. The rapid decrease in the vibration amplitude is a result of the big damping forces. These forces decrease the peak strain value. Decaying of the vibration amplitude with time is shown in Fig. 15.

One-term series nonlinear solution and experimental results obtained for specimen II are shown in Fig. 16. A simple approximation to the prediction of the strain at the center of the plate and response frequency is presented and compared with the experimental results. A discrepancy between the theoretical and experimental results is observed for the time history. This discrepancy shows the effect of higher vibration modes on the plate response. One-term series nonlinear solution and experimental results of specimen I for the second load case are shown in Fig. 17. In this figure there is a difference between the theoretical and experimental results. The strains obtained in the second load case are bigger than the strains obtained in the first loading condition. This is the result of the big deflection in the second load case. The difference between the experimental and theoretical results in the second load case is bigger than the difference between the experimental and theoretical results in the first load case because the assumptions have many more effects on the results in the second load case.

V. Conclusions

This paper presents a theoretical analysis and correlation with numerical and experimental results of the strain time histories of laminated composite plates exposed to normal blast shock waves. The blast wave is assumed to be exponentially decaying with time and either uniformly distributed on the plate surface or sinusoidal varying with coordinates. Two different lamina configurations are investigated. The equation of motion of the plate is solved using the Runge–Kutta–Verner method and correlated with the experimental and ANSYS finite element results for the seven-layered composite plate. The following conclusions apply to the case of laminated plates with fully fixed boundary conditions as considered herein.

The blast-pressure measurements on the plate show that the character of the pressure variation is strongly dependent on the distance from the open end of the tube to the target plate. For example, if we decrease this distance about three times, the peak pressure on the plate increases approximately 10 times. Furthermore, the ratio of the positive peak pressure to the negative peak pressure increases with the increasing distance. The pressure distribution on the plate has a sinusoidal variation for the cases of low distance. On the other hand, the spatial variation of the pressure becomes more uniform as the distance increases.

From the time response curves theoretical and numerical results are in a good agreement in the linear range. Theoretical analysis results show that the number of terms is an effective parameter in the geometrically nonlinear solution. The predicted peak strain value and response frequency obtained from nine-term series solution is well-correlated with the numerical result in the nonlinear range. Strains and frequency obtained from theoretical and numerical analyses are correlated with the experimental results. Response frequencies obtained from theoretical and numerical methods are in agreement. The discrepancy between the peak strains obtained from experimental and the other methods is because of the assumptions, which are made in the analyses. A simple approximation to the prediction of the strain at the center of the plate and response frequency is achieved using one-term series in the analysis. The decaying shown in the experimental results does not appear in the results of the analyses. A decaying parameter can be calculated from the long-time response curves and may be used in the analyses, but this procedure is not shown in this study. The discrepancy between the experimental and theoretical results caused by the assumptions is much more clear for the low-distance case. In this case the big strains and displacements occur in comparison to the first loading condition; therefore, the assumptions become more significant factors on the plate response. In the second load case the plate moves more rapidly because of the blast load with high velocity, and therefore the structural damping becomes more significant factor restricting the plate response. Finally, if the frequencies and peak strains are considered, an agreement is found between the experimental results and the others in the first loading condition. The numerical solution procedure requires much more computer time than the approximate theoretical solution procedure. Thus the theoretical solution may be used for providing material in the preliminary design stage.

The structural damping and hygro-thermal effects may be interesting in the aspect of the dynamic response of plate. The stiffener and cutout effects on the dynamic behavior of the plate can be studied by the use of this method. These will be the topics of the next studies.

Appendix: Derivation of the Equations of Motion

Substituting the constitutive equations in Eq. (4), we obtain the equations of motion as

$$-\frac{\partial N_x}{\partial x}-\frac{\partial N_{xy}}{\partial y}-q_x-\bar{m}\ddot{u}^0=0 \tag{A1}$$

$$-\frac{\partial N_y}{\partial y}-\frac{\partial N_{xy}}{\partial x}-q_y-m\ddot{v}^0=0 \tag{A2}$$

$$\begin{aligned}&-\frac{\partial^2 M_x}{\partial x^2}-\frac{\partial^2 M_y}{\partial y^2}-2\frac{\partial^2 M_{xy}}{\partial x\partial y}-\left(\frac{\partial N_x}{\partial x}+\frac{\partial N_{xy}}{\partial y}\right)\frac{\partial w^0}{\partial x}\\&-\left(\frac{\partial N_y}{\partial y}+\frac{\partial N_{xy}}{\partial x}\right)\frac{\partial w^0}{\partial y}-\left(N_x\frac{\partial^2 w^0}{\partial x^2}+N_{xy}\frac{\partial^2 w^0}{\partial x\partial y}\right.\\&\left.+N_y\frac{\partial^2 w^0}{\partial y^2}\right)-q_z-\bar{m}\ddot{w}^0=0\end{aligned} \tag{A3}$$

where

$$\begin{bmatrix}N_x\\N_y\\N_{xy}\end{bmatrix}=\begin{bmatrix}A_{11}&A_{12}&A_{16}\\A_{12}&A_{22}&A_{26}\\A_{16}&A_{26}&A_{66}\end{bmatrix}\begin{bmatrix}\varepsilon_x^0\\\varepsilon_y^0\\\varepsilon_{xy}^0\end{bmatrix}+\begin{bmatrix}B_{11}&B_{12}&B_{16}\\B_{12}&B_{22}&B_{26}\\B_{16}&B_{26}&B_{66}\end{bmatrix}\begin{bmatrix}\kappa_x\\\kappa_y\\\kappa_{xy}\end{bmatrix} \tag{A4}$$

$$\begin{bmatrix}M_x\\M_y\\M_{xy}\end{bmatrix}=\begin{bmatrix}B_{11}&B_{12}&B_{16}\\B_{12}&B_{22}&B_{26}\\B_{16}&B_{26}&B_{66}\end{bmatrix}\begin{bmatrix}\varepsilon_x^0\\\varepsilon_y^0\\\varepsilon_{xy}^0\end{bmatrix}+\begin{bmatrix}D_{11}&D_{12}&D_{16}\\D_{12}&D_{22}&D_{26}\\D_{16}&D_{26}&D_{66}\end{bmatrix}\begin{bmatrix}\kappa_x\\\kappa_y\\\kappa_{xy}\end{bmatrix} \tag{A5}$$

Here, terms in the matrices are

$$A_{ij}=\sum_{k=1}^{n}(Q_{ij})_k(h_k-h_{k-1})$$

$$B_{ij}=\frac{1}{2}\sum_{k=1}^{n}(Q_{ij})_k\left(h_k^2-h_{k-1}^2\right)$$

$$D_{ij}=\frac{1}{3}\sum_{k=1}^{n}(Q_{ij})_k\left(h_k^3-h_{k-1}^3\right)$$

Using the constitutive equations and strain-displacement relations, Eqs. (A1–A3) can be written in terms of displacements as

$$\begin{aligned}L_{11}u^0+L_{12}v^0+L_{13}w^0+N_1(w^0)+\bar{m}\ddot{u}^0-q_x=0\\L_{21}u^0+L_{22}v^0+L_{23}w^0+N_2(w^0)+\bar{m}\ddot{v}^0-q_y=0\\L_{31}u^0+L_{32}v^0+L_{33}w^0+N_3(u^0,v^0,w^0)+\bar{m}\ddot{u}^0-q_z=0\end{aligned} \tag{A6}$$

where

$$L_{11}=-A_{11}\frac{\partial^2}{\partial x^2}-2A_{16}\frac{\partial^2}{\partial x\partial y}-A_{66}\frac{\partial^2}{\partial y^2}$$

$$L_{12}=-(A_{12}+A_{66})\frac{\partial^2}{\partial x\partial y}-A_{16}\frac{\partial^2}{\partial x^2}-A_{26}\frac{\partial^2}{\partial y^2}$$

$$L_{13}=3B_{16}\frac{\partial^3}{\partial x^2\partial y}+(B_{12}+2B_{66})\frac{\partial^3}{\partial x\partial y}+B_{11}\frac{\partial^3}{\partial x^3}+B_{26}\frac{\partial^3}{\partial y^3}$$

$$L_{21}=-(A_{12}+A_{66})\frac{\partial^2}{\partial x\partial y}-A_{16}\frac{\partial^2}{\partial x^2}-A_{26}\frac{\partial^2}{\partial y^2}$$

$$L_{22}=-A_{66}\frac{\partial^2}{\partial x^2}-A_{22}\frac{\partial^2}{\partial y^2}-2A_{26}\frac{\partial^2}{\partial x\partial y}$$

$$L_{23}=(B_{12}+2B_{66})\frac{\partial^3}{\partial y\partial x^2}+B_{22}\frac{\partial^3}{\partial y^3}+3B_{26}\frac{\partial^3}{\partial x\partial y^2}+B_{16}\frac{\partial^3}{\partial x^3}$$

$$L_{31}=-B_{11}\frac{\partial^3}{\partial x^3}-3B_{16}\frac{\partial^3}{\partial x^2\partial y}-(B_{12}+2B_{66})\frac{\partial^3}{\partial x\partial y^2}-B_{26}\frac{\partial^3}{\partial y^3}$$

$$L_{32}=-B_{16}\frac{\partial^3}{\partial x^3}-(B_{12}+2B_{66})\frac{\partial^3}{\partial x^2\partial y}-3B_{26}\frac{\partial^3}{\partial x\partial y^2}-B_{22}\frac{\partial^3}{\partial y^3}$$

$$\begin{aligned}L_{33}=&D_{11}\frac{\partial}{\partial x^4}+6D_{16}\frac{\partial^4}{\partial x^3\partial y}+(2D_{12}+4D_{66})\frac{\partial^4}{\partial x^2\partial y^2}\\&+4D_{26}\frac{\partial^4}{\partial x\partial y^3}+D_{22}\frac{\partial^4}{\partial y^4}\end{aligned}$$

$$\begin{aligned}N_1(w^0)=&-A_{11}\frac{\partial w^0}{\partial x}\frac{\partial^2 w^0}{\partial x^2}-(A_{12}+A_{66})\frac{\partial w^0}{\partial y}\frac{\partial^2 w^0}{\partial x\partial y}\\&-A_{16}\frac{\partial w^0}{\partial y}\frac{\partial^2 w^0}{\partial x^2}-2A_{16}\frac{\partial w^0}{\partial x}\frac{\partial^2 w^0}{\partial x\partial y}-A_{26}\frac{\partial w^0}{\partial y}\frac{\partial^2 w^0}{\partial y^2}\\&-A_{66}\frac{\partial w^0}{\partial x}\frac{\partial^2 w^0}{\partial y^2}\end{aligned}$$

$$\begin{aligned}N_2(w^0)=&-(A_{12}+A_{66})\frac{\partial w^0}{\partial x}\frac{\partial^2 w^0}{\partial x\partial y}-A_{22}\frac{\partial w^0}{\partial y}\frac{\partial^2 w^0}{\partial y^2}\\&+2A_{26}\frac{\partial w^0}{\partial y}\frac{\partial^2 w^0}{\partial x\partial y}-A_{26}\frac{\partial w^0}{\partial x}\frac{\partial^2 w^0}{\partial Y^2}-A_{16}\frac{\partial w^0}{\partial x}\frac{\partial^2 w^0}{\partial x^2}\\&-A_{66}\frac{\partial w^0}{\partial y}\frac{\partial^2 w^0}{\partial x^2}-A_{22}\frac{\partial w^0}{\partial y}\frac{\partial^2 w^0}{\partial y^2}\end{aligned}$$

$$\begin{aligned}N_3(u^0,v^0,w^0)=&2(B_{66}-B_{12})\left(\frac{\partial^2 w^0}{\partial x\partial y}\right)^2+(B_{22}-B_{12})\left(\frac{\partial^2 w^0}{\partial y^2}\right)^2\\&-4B_{66}\left(\frac{\partial w^0}{\partial y}\frac{\partial^3 w^0}{\partial y\partial x^2}\right)+(B_{22}-B_{12})\left(\frac{\partial w^0}{\partial y}\frac{\partial^3 w^0}{\partial y^3}\right)\\&+2(B_{12}-B_{66})\left(\frac{\partial^2 w^0}{\partial x^2}\frac{\partial^2 w^0}{\partial y^2}\right)-A_{11}\left(\frac{\partial^2 u^0}{\partial x^2}\frac{\partial w^0}{\partial x}\right)\\&-\left(\frac{3A_{11}}{2}\right)\left(\frac{\partial w^0}{\partial x}\right)^2\frac{\partial^2 w^0}{\partial x^2}-(A_{12}+A_{66})\left(\frac{\partial^2 v^0}{\partial y\partial x}\frac{\partial w^0}{\partial x}\right)\\&-2(A_{12}+2A_{66})\left(\frac{\partial w^0}{\partial y}\frac{\partial^2 w^0}{\partial y\partial x}\frac{\partial w^0}{\partial x}\right)-2A_{16}\left(\frac{\partial^2 u^0}{\partial x\partial y}\frac{\partial w^0}{\partial x}\right)\\&-A_{16}\left(\frac{\partial^2 v^0}{\partial x^2}\frac{\partial w^0}{\partial x}\right)-2A_{16}\left(\frac{\partial^2 w^0}{\partial x^2}\frac{\partial w^0}{\partial y}\frac{\partial w^0}{\partial x}\right)\\&-3A_{16}\left(\frac{\partial w^0}{\partial x}\right)^2\frac{\partial^2 w^0}{\partial y\partial x}-A_{26}\left(\frac{\partial^2 v^0}{\partial y^2}\frac{\partial w^0}{\partial x}\right)\\&-3A_{26}\left(\frac{\partial w^0}{\partial y}\frac{\partial^2 w^0}{\partial y^2}\frac{\partial w^0}{\partial x}\right)-A_{66}\left(\frac{\partial^2 u^0}{\partial y^2}\frac{\partial w^0}{\partial x}\right)\\&-\left(A_{66}+\frac{A_{12}}{2}\right)\left(\frac{\partial w^0}{\partial x}\right)^2\frac{\partial^2 w^0}{\partial y^2}-(A_{12}+A_{66})\left(\frac{\partial^2 u^0}{\partial x\partial y}\frac{\partial w^0}{\partial y}\right)\\&-A_{22}\left(\frac{\partial^2 v^0}{\partial y^2}\frac{\partial w^0}{\partial y}\right)-\left(\frac{3A_{22}}{2}\right)\left(\frac{\partial w^0}{\partial y}\right)^2\frac{\partial^2 w^0}{\partial y^2}\\&-A_{26}\left(\frac{\partial^2 u^0}{\partial y^2}\frac{\partial w^0}{\partial y}\right)-2A_{26}\left(\frac{\partial^2 v^0}{\partial x\partial y}\frac{\partial w^0}{\partial y}\right)\\&-4A_{26}\left(\frac{\partial^2 w^0}{\partial x\partial y}\right)\left(\frac{\partial w^0}{\partial y}\right)^2-A_{16}\left(\frac{\partial^2 u^0}{\partial x^2}\frac{\partial w^0}{\partial y}\right)\end{aligned}$$

$$
\begin{aligned}
&- A_{66}\left(\frac{\partial^2 v^0}{\partial x^2}\frac{\partial w^0}{\partial y}\right) - \left(A_{66} + \frac{A_{12}}{2}\right)\left(\frac{\partial w^0}{\partial y}\right)\frac{\partial^2 w^0}{\partial x^2} \\
&- A_{11}\left(\frac{\partial^2 w^0}{\partial x^2}\frac{\partial u^0}{\partial x}\right) - A_{12}\left(\frac{\partial v^0}{\partial y}\frac{\partial^2 w^0}{\partial y^2}\right) - A_{16}\left(\frac{\partial u^0}{\partial y}\frac{\partial^2 w^0}{\partial x^2}\right) \\
&- A_{16}\left(\frac{\partial v^0}{\partial x}\frac{\partial^2 w^0}{\partial x^2}\right) - A_{12}\left(\frac{\partial u^0}{\partial x}\frac{\partial^2 w^0}{\partial y^2}\right) - A_{22}\left(\frac{\partial v^0}{\partial y}\frac{\partial^2 w^0}{\partial y^2}\right) \\
&- A_{26}\left(\frac{\partial u^0}{\partial y}\frac{\partial^2 w^0}{\partial y^2}\right) - A_{26}\left(\frac{\partial v^0}{\partial x}\frac{\partial^2 w^0}{\partial y^2}\right) - 2A_{16}\left(\frac{\partial u^0}{\partial x}\frac{\partial^2 w^0}{\partial x \partial y}\right) \\
&- 2A_{26}\left(\frac{\partial v^0}{\partial y}\frac{\partial^2 w^0}{\partial x \partial y}\right) - 2A_{66}\left(\frac{\partial u^0}{\partial y}\frac{\partial^2 w^0}{\partial x \partial y}\right) \\
&- 2A_{66}\left(\frac{\partial v^0}{\partial x}\frac{\partial^2 w^0}{\partial x \partial y}\right)
\end{aligned}
$$

with the boundary conditions

$$
\begin{aligned}
&u^0(0, y, t) = u^0(a, y, t) = u^0(x, 0, t) = u^0(x, b, t) = 0 \\
&\frac{\partial u^0}{\partial x}(0, y, t) = \frac{\partial u^0}{\partial x}(a, y, t) = \frac{\partial u^0}{\partial y}(x, 0, t) = \frac{\partial u^0}{\partial y}(x, b, t) = 0 \\
&v^0(0, y, t) = v^0(a, y, t) = v^0(x, 0, t) = v^0(x, b, t) = 0 \\
&\frac{\partial v^0}{\partial x}(0, y, t) = \frac{\partial v^0}{\partial x}(a, y, t) = \frac{\partial v^0}{\partial y}(x, 0, t) = \frac{\partial v^0}{\partial y}(x, b, t) = 0 \\
&w^0(0, y, t) = w^0(a, y, t) = w^0(x, 0, t) = w^0(x, b, t) = 0 \\
&\frac{\partial w^0}{\partial x}(0, y, t) = \frac{\partial w^0}{\partial x}(a, y, t) = \frac{\partial w^0}{\partial y}(x, 0, t) = \frac{\partial w^0}{\partial y}(x, b, t) = 0
\end{aligned}
\tag{A7}
$$

and initial conditions

$$
\begin{aligned}
&u^0(x, y, 0) = 0, \qquad v^0(x, y, 0) = 0, \qquad w^0(x, y, 0) = 0 \\
&\dot{u}^0(x, y, 0) = 0, \qquad \dot{v}^0(x, y, 0) = 0, \qquad \dot{w}^0(x, y, 0) = 0
\end{aligned}
\tag{A8}
$$

Acknowledgments

This study was supported in part by a grant from the Istanbul Technical University Research Fund and Turkish Airlines. The authors thank Turkish Airlines Cabin Quality Manager Ali Eser for assistance in manufacturing the composites.

References

[1]Pilato, L. A., and Michna, M. J., *Advanced Composite Materials*, Springer–Verlag, New York, 1994, pp. 157–185.

[2]Hopkinson, B., British Ordnance Board Minutes, Rept. 13565, British Ordnance Office, London, 1915.

[3]Houlston, R., Slater, J. E., Pegg, N., and DesRochers, C. G., "On Analysis of Structural Response of Ship Panels Subjected to Air Blast Loading," *Computers and Structures*, Vol. 21, No. 1/2, 1985, pp. 273–289.

[4]Houlston, R., and DesRochers, C. G., "Nonlinear Structural Response of Ship Panels Subjected to Air Blast Loading," *Computers and Structures*, Vol. 26, No. 1/2, 1987, pp. 1–15.

[5]Gupta, A. D., Gregory, F. H., Bitting, R. L., and Bhattacharya, S., "Dynamic Analysis of an Explosively Loaded Hinged Rectangular Plate," *Computers and Structures*, Vol. 26, No. 1/2, 1987, pp. 339–344.

[6]Beshara, F. B. A., "Modeling of Blast Loading on Aboveground Structures—I. General Phenomenology and External Blast," *Computers and Structures*, Vol. 51, No. 5, 1994, pp. 585–596.

[7]Olson, M. D., "Efficient Modeling of Blast Loaded Stiffened Plate and Cylindrical Shell Structures," *Computers and Structures*, Vol. 40, No. 5, 1991, pp. 1139–1149.

[8]Nurick, G. N., Olson, M. D., Fagnan, J. R., and Levin, A., "Deformation and Tearing of Blast-Loaded Stiffened Square Plates," *International Journal of Impact Engineering*, Vol. 16, No. 2, 1995, pp. 273–291.

[9]Wiernicki, C. J., Liem, F., Woods, G. D., and Furio, A. J., "Structural Analysis Methods for Lightweight Metallic Corrugated Core Sandwich Panels Subjected to Blast Loads," *Naval Engineers Journal*, Vol. 101, No. 5, 1990, pp. 192–203.

[10]Librescu, L., and Nosier, A., "Response of Laminated Composite Flat Panels to Sonic Boom and Explosive Blast Loadings," *AIAA Journal*, Vol. 28, No. 2, 1990, pp. 345–352.

[11]Türkmen, H. S., and Mecitoglu, Z., "Dynamic Behavior of Laminated Composite Plate Subjected to Shock Loading," *First International Aerospace and Advanced Technologies Symposium*, edited by Z. Mecitoglu, Vol. 1, Istanbul Technical Univ., Istanbul, Turkey, 1995, pp. 475–484.

[12]Türkmen, H., Mecitoglu, Z., and Borat, O., "Nonlinear Structural Response of Laminated Composite Panels Subjected to Blast Loadings," *Mathematical and Computational Applications*, Vol. 1, No. 1, 1996, pp. 126–133.

[13]Türkmen, H., "Dynamic Response of Laminated Composite Panels Subjected to Blast Loading," Ph.D. Dissertation, Aerospace Engineering Dept., Istanbul Technical Univ., Istanbul, Turkey, 1998.

[14]Mecitoglu, Z., "Governing Equations of a Stiffened Laminated Inhomogeneous Conical Shell," *AIAA Journal*, Vol. 34, No. 10, 1996, pp. 2118–2125.

[15]Stein, M., "Nonlinear Theory for Plates and Shells Including the Effects of Transverse Shearing," *AIAA Journal*, Vol. 24, No. 9, 1986, pp. 1537–1544.

[16]Chawla, K. K., *Composite Materials*, Springer–Verlag, New York, 1987, pp. 204–258.

G. A. Kardomateas
Associate Editor